

Article

Role of Lewis Acid Metal Centers in Metal–Organic Frameworks for Ultrafast Reduction of 4-Nitrophenol

Jagannath Panda ^{1,†}, Soumya Prakash Biswal ^{2,†}, Himanshu Sekhar Jena ^{3,*}, Arijit Mitra ⁴, Raghabendra Samantray ^{1,2,*} and Rojalin Sahu ^{1,*}

¹ Future Materials Laboratory, Department of Chemistry, School of Applied Sciences, KIIT Deemed to Be University, Bhubaneswar 751024, India; jagannath.panda777@gmail.com

² School of Chemical Technology, KIIT Deemed to Be University, Bhubaneswar 751024, India; biswalsoumya86@gmail.com

³ Department of Chemistry, Ghent University, Krijgslaan 281-S3 B, 9000 Ghent, Belgium

⁴ Institute of Physics, Bhubaneswar 751005, India; arijit01@gmail.com

* Correspondence: hsjena@gmail.com (H.S.J.); rsamantray@gmail.com (R.S.); rsahufch@kiit.ac.in (R.S.)

† These authors contributed equally to this work.

Abstract: Metal–Organic Frameworks (MOFs) can be a good alternative to conventional catalysts because they are non-toxic and can be selective without compromising efficiency. Nano MOFs such as UiO-66 have proven themselves to be competitive in the catalytic family. In this study, we report the excellent catalytic behavior of UiO-66 MOF in the reduction of a model reaction: 4-Nitrophenol (4-NP) to 4-Aminophenol (4-AP) over MOF-5 (Zn-BDC) and MIL-101 (Fe-BDC). Nano UiO-66 crystals were synthesized by a hydrothermal process and characterized by Powder X-ray Diffraction, Diffused Reflectance UV-Vis spectroscopy, Scanning Electron Microscopy, and Transmission Electron Microscopy. The catalysts' performance during the hydrogenation reduction reaction from 4-NP to 4-AP was investigated in the presence of a reducer, NaBH₄. The UiO-66 nano crystals exhibited excellent catalytic behavior owing to its large surface area and Lewis acidic nature at the metal nodes. Furthermore, UiO-66 showed excellent recyclability behavior, verified during repeated consecutive use in a sequence. The catalyst yielded similar catalytic behavior during the reduction of nitrophenols at each cycle, which is a novel finding.

Keywords: nano-metal organic frameworks (MOFs); UiO-66; catalyst; reduction reactions; reusability



Citation: Panda, J.; Biswal, S.P.; Jena, H.S.; Mitra, A.; Samantray, R.; Sahu, R. Role of Lewis Acid Metal Centers in Metal–Organic Frameworks for Ultrafast Reduction of 4-Nitrophenol. *Catalysts* **2022**, *12*, 494. <https://doi.org/10.3390/catal12050494>

Academic Editors: Antal Csampai and Tamás Jernei

Received: 5 March 2022

Accepted: 20 April 2022

Published: 29 April 2022

Publisher's Note: MDPI stays neutral with regard to jurisdictional claims in published maps and institutional affiliations.



Copyright: © 2022 by the authors. Licensee MDPI, Basel, Switzerland. This article is an open access article distributed under the terms and conditions of the Creative Commons Attribution (CC BY) license (<https://creativecommons.org/licenses/by/4.0/>).

1. Introduction

Metal Organic Frameworks (MOFs) have been center-stage in material science research due to their numerous applications in luminescence-based sensing [1], catalysis [2,3], adsorptions [4], and separation [5]. Recently, they have been synthesized at particle sizes of 5–50 nm in diameter [6], colloquially known as nano-particles, which has enabled them for use in catalytic applications [7]. The origin of the broad status of MOFs lies in their porous crystalline nature and tunability, which lends them to several uses [8]. In MOFs, metal ions are connected by organic linkers to form coordination networks. Generally, MOFs are crystalline solids. MOFs are well known for their enormous porosity (pore volumes up to 6000 m³/g) [9], ultralow densities [10], high surface area [11], and high metal ion concentrations in the nano porous matrix [12]. These properties make them well matched for catalytic applications, and they also have high selectivity [13]. In addition, they are recognized for their relatively easy chemical synthesis and for being inexpensive and environmental-friendly, as most of them are non-toxic [14].

As catalysts, MOFs are considered superior to noble metal nano particles for the reason that they carry a high concentration of metal ions that are well separated from each other through coordination bonds with their organic linkers. The inorganic clusters behave as unsaturated Lewis acids, which facilitate catalytic processes [15,16]. Nanoporous

MOFs, with their exceptional surface area, help in converting reactants to products with minimal reaction time and outstanding recyclability [17]. Furthermore, MOFs have great potential as heterogeneous catalysts that can be utilized with ease in reaction sites with variable activity and selectivity [18]. Among them, UiO-66 nano-MOFs stand out as robust materials as they can withstand harsh conditions. UiO-66 has been used as an efficient catalyst in the cyanosilylation of benzaldehyde via its active Lewis acidic sites [19]. Though UiO-66 and other MOFs are widely utilized for their catalytic activities, in most cases they are alloyed with other matrices for optimum results. Pd nanoparticle-loaded MOF Pd@Zn₂(azoBDC)₂(dabco) have been used to catalyze the reduction of nitro aromatics to amines with a good conversion rate and excellent recyclability [20]. Au nano particles have been alloyed with amine-functionalized UiO-66 and have been successfully used as a catalyst for selective tandem catalytic reactions [21]. Ag–Pd nano particle composites with N-doped porous carbon and UiO-66 MOFs have shown excellent reduction reactions on nitroarenes [22]. To increase the surface area and pore sizes and to improve their catalytic activity, alloys of Au–Pd has been encapsulated in amino-functionalized UiO-66 MOF [23]. Au-loaded metal nano particles in MOF-3 have been used for the reduction of 4-Nitrophenol in the presence NaBH₄ [24]. Furthermore, Au nano particle-encapsulated ZIF-8, Au@ZIF-8(Zn,Cu), has been used for the reduction of nitroarenes [25]. Composites of Fe₃O₄@MIL-100(Fe)–Pt containing Fe and Pt have been used for the reduction of nitrophenols; these composites have magnetic properties that make them suitable for reuse for many cycles, as they can be easily recovered [26]. A 2D Cu-BDC MOF consisting of Cu metal has been used for the reduction of nitrophenols [27].

Encouraged by the catalytic usability of our synthesized UiO-66 MOF, we have examined the catalytic properties of the only UiO-66 nano MOF that has no expensive metal nano particles on a model catalytic reaction: 4-Nitrophenol (hereafter referred to as 4-NP) to 4-Aminophenol (hereafter referred to as 4-AP). We also compared the catalytic behavior of MOF-5 (Zn-BDC) and MIL-101 (Fe-BDC). The catalytic behavior was evaluated by time-dependent spectroscopic measurements at variable catalyst concentrations. Considering the robust behavior of UiO-66, we performed the catalytic recyclability test following the same experimental conditions. Our assumption did pan out, with an exceptional, near-perfect catalytic activity for up to four cycles in a sequence.

2. Materials and Methods

2.1. Synthesis of the UiO-66 MOF

All the starting materials and solvents were purchased from commercial suppliers (Alfa Aesar, Haverhill, MA, USA, Across Organics, Geel, Belgium and Tokyo Chemical Industry, Inc., Tokyo, Japan), and used without further purification. UiO-66 was prepared following the procedure in the literature [28,29] with slight modifications. In a typical method for the synthesis of UiO-66 MOF, ZrCl₄ is used as the metal source and Benzene-1,4-dicarboxylic acid, BDC-H₂, is used as the linker at a 1:1 ratio. These two precursors were mixed in a screw cap glass vessel and dissolved in DMF. Then, the mixture was kept at 110 °C for 24 h and cooled. In the solution, a white-color powder was generated. This was centrifuged to separate the white solid and washed repeatedly with DMF to remove the unreacted reactants. Then, the solvent exchange was performed by soaking in DCM for 72 h and drying in a vacuum oven at 60 °C for 1 h. This powder was used for further characterization. The procedure for the synthesis of the MIL-101(Fe) and MOF-5(Zn-BDC) are given in the Supplementary Materials File.

2.2. Characterization of the UiO-66 MOF

The Powder X-ray Diffraction (PXRD) technique was used to verify the crystalline properties of the synthesized UiO-66 framework material. The PXRD was collected using a Bruker APEXII X-ray Diffractometer ($\lambda = 1.54056 \text{ \AA}$). Measurements were carried out in the 2θ values in the range of 5–50°. This experimentally observed PXRD pattern was compared with the simulated patterns of previously reported structures [30]. An Agilent

Cary 5000 UV-Vis-NIR spectrometer was used to study the Diffused reflectance UV-Visible spectra. The catalytic reaction was carried out with a Thermo scientific Orion 8000UV-Visible spectrometer. Fourier-transform infrared (FT-IR) spectra were obtained in a Nicolet iS10 system in the frequency range of 4000–400 cm⁻¹. The Thermo gravimetric analysis (TGA) experiment was carried out in the temperature range of 30–800 °C on a Hitachi STA-7200 instrument under a N₂ atmosphere at a heating rate of 10 °C min⁻¹. Scanning Electron Microscopy (SEM) images were obtained with a ZEISS Scanning Electron Microscope with a tungsten filament as an electron source operating at 10–20 kV. HR-TEM images were captured by a TEM Microscope (JEOL-2010). Electrospray ionization mass spectrometry (ESI-MS) spectra were recorded on a Bruker Daltonics MicroTOF-Q-II mass spectrometer. The ¹H analyses were performed on a Bruker Advance 300 MHz spectrometer.

2.3. Reduction of 4-Nitrophenol

The catalytic efficiency of the UiO-66, MOF-5 (Zn-BDC), and MIL-101 (Fe-BDC) MOFs were evaluated in the reduction reaction of 4-NP to 4-AP. The catalytic reaction was carried out in a quartz cuvette by in situ monitoring of UV-Visible changes at a wavelength of 400 nm. Sodium borohydride (NaBH₄) was used as a reducer in the reduction reaction. The catalytic solution was prepared by adding 1 mg of any of the MOFs (UiO-66), MOF-5 (Zn-BDC), and MIL-101 (Fe-BDC)) in 1 mL of water. The solution was sonicated for 3 min to ensure that a homogeneous mixture was prepared. To study the reduction process using our synthesized catalyst, 2 mL of 0.3 mM of 4-Nitrophenol was taken in a cuvette made up of quartz with a 1 cm path length. In addition to this, 0.5 mL of aqueous solution of sodium borohydride was added. Then, the solution was mixed thoroughly, followed by the addition of the catalyst solutions in different quantities—UiO-66 (0.5, 0.3, 0.2 mg/mL) and 0.5 mL of MOF-5 (Zn-BDC) and MIL-101 (Fe-BDC)—to the quartz cuvette. The UV-Visible spectral observations were made at various time intervals till the end of the reaction—the disappearance of the peak at 400 nm. The sample was cleaned and dried after the completeness of the reaction to re-use for further catalytic activity. The catalyst was reused for four similar tests to ensure the recyclability of the catalyst. We have measured the value of the rate constant k by measuring the absorbance at 400 nm (Å) with the help of a UV-Vis spectrophotometer as a function of time. The percentage of conversion as well as the parameters for the reaction kinetics was also evaluated.

3. Results and Discussion

3.1. Powder X-ray Diffraction Study

The Powder XRD analysis of the synthesized MOF was performed to verify the synthesis of the sample. The synthesis of the MOF, UiO-66, was confirmed by comparison with the simulated pattern. The PXRD pattern obtained for this synthesized UiO-66 MOF was matched well with the simulated pattern, as shown in Figure 1 [31]. From this study, it was concluded that the sample was synthesized properly and the MOF structure was confirmed. The PXRD patterns for MIL-101(Fe) and MOF-5(Zn-BDC) are shown in Figure S1.

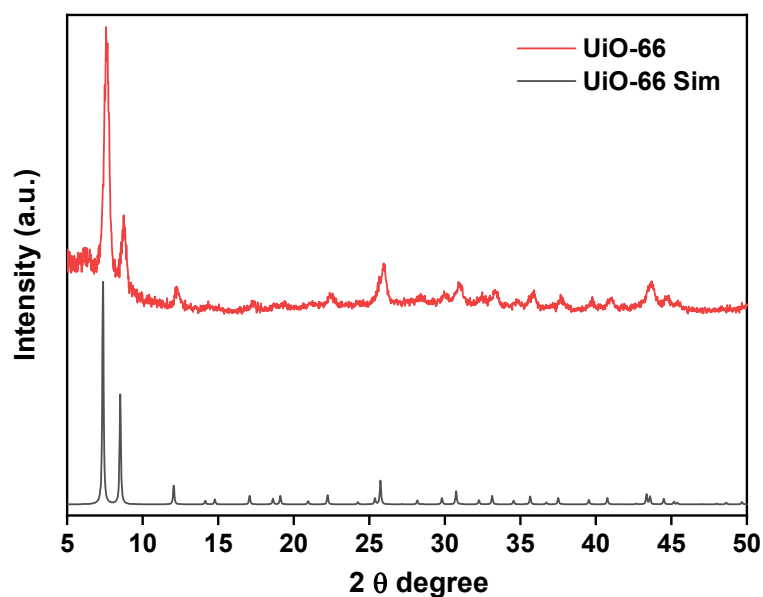


Figure 1. PXRD patterns of UiO-66.

3.2. Diffused Reflectance UV-Visible Spectra

The diffused reflectance (DR) UV-Visible spectra of the UiO-66 compound is shown in Figure 2. UiO-66 shows no absorption in the Visible region, which can be seen from the figure. Furthermore, it attained the expected color for the sample, which is white [31]. A peak present at around 320 nm was attributed to ligand-to-metal charge transfer (LMCT) spectra. This spectra is mainly due to the presence of the functional groups and aromatic rings [21].

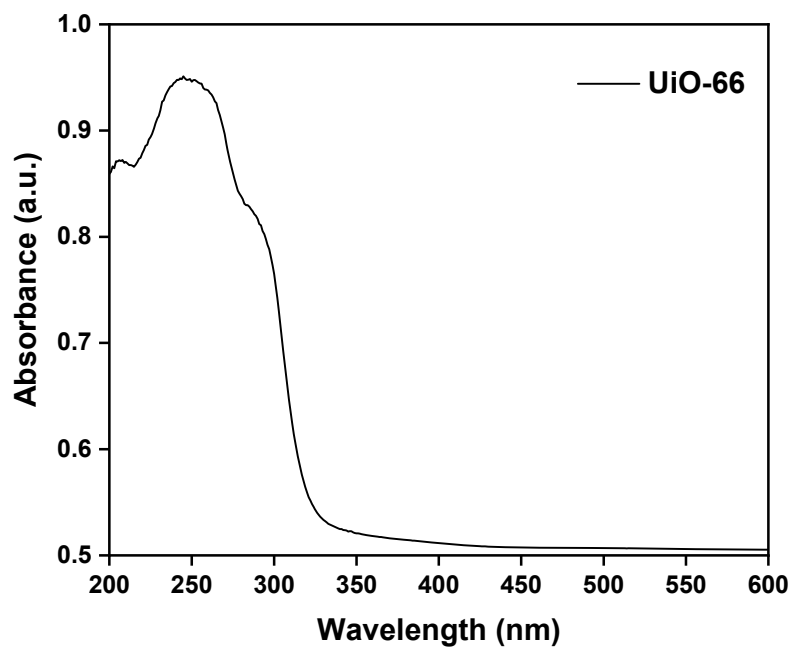


Figure 2. Diffused reflectance UV-Vis spectra of UiO-66.

3.3. Fourier Transform Infrared Spectra (FT-IR)

The FT-IR spectra of UiO-66 is shown in Figure 3. The out-of-plane and in-plane stretching modes of the -COOH groups in the UiO-66 were shown as a doublet at 1590 cm^{-1} and 1400 cm^{-1} . The vibrational modes of the Zr-O₂ appeared at 723 cm^{-1} , 650 cm^{-1} , and 550 cm^{-1} [32].

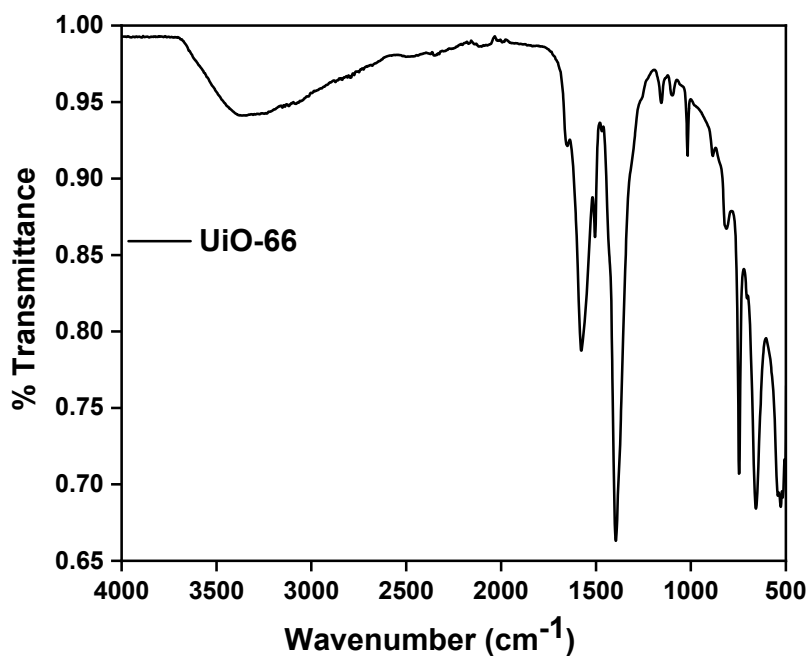


Figure 3. FT-IR spectra of UiO-66.

3.4. Specific Surface Area Analysis

Since MOFs are known to be porous materials, N₂ isotherms at 77 K were measured on the activated samples of the synthesized MOF. Typical isotherms of type-IV were observed for the UiO-66, which can be seen in Figure 4. This synthesized MOF was microporous in nature, which was confirmed by the BET measurement. The predominant presence of microporosity in the MOF structure was confirmed from the N₂ uptake at the region of low pressure ($P/P_0 < 0.2$) [33]. Furthermore, the microporosity was confirmed from the adsorption–desorption isotherm forming the hysteresis loop. Based on these results, we ascertained that the synthesized MOF was highly porous.

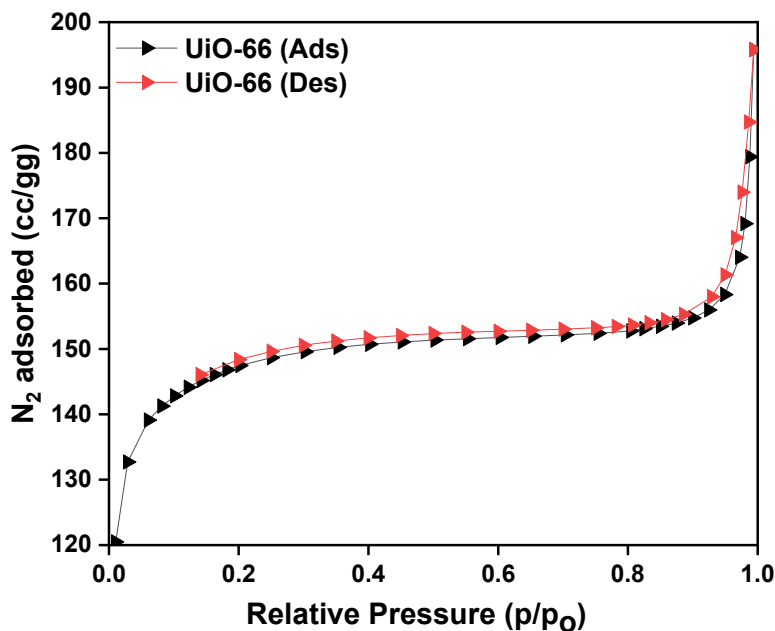


Figure 4. N₂ adsorption isotherm graphs of UiO-66.

3.5. Thermo Gravimetric Analysis (TGA)

To study the thermal stability of our synthesized MOF UiO-66, thermo gravimetric analysis (TGA) was carried out and is shown in Figure 5. The sample was analyzed in the temperature ranges of 350 °C to 500 °C. The UiO-66 sample was stable for up to 500 °C, which matches very well with previously reported results [34].

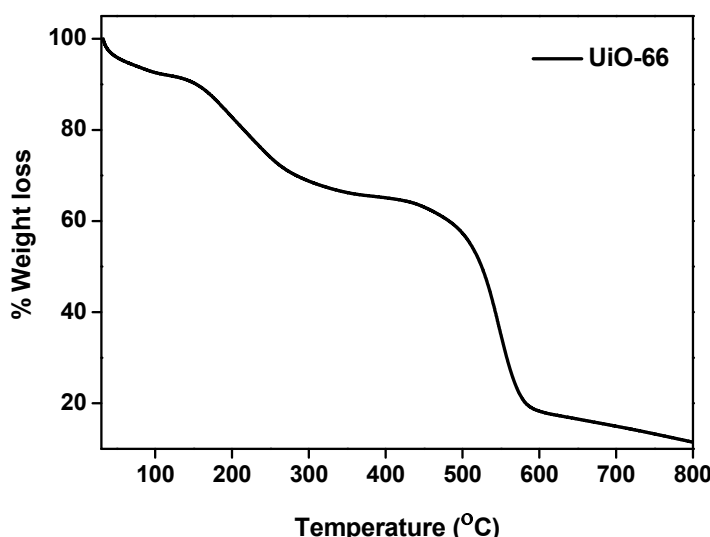


Figure 5. TGA graphs of UiO-66.

3.6. Scanning Electron Microscopy (SEM) and Transmission Electron Microscopy (TEM)

The synthesized MOF UiO-66 was characterized to study its surface morphology by SEM and TEM. The images obtained from the SEM is depicted in Figure 6a. The TEM image of the MOF is shown in Figure 6b. The average crystal sizes of the UiO-66 crystals were in the range of 100–200 nm, which was confirmed by the SEM analysis. A hollow structure in the crystals was found from the TEM image, indicating the presence of meso pores, as shown in Figure 6b [35,36].

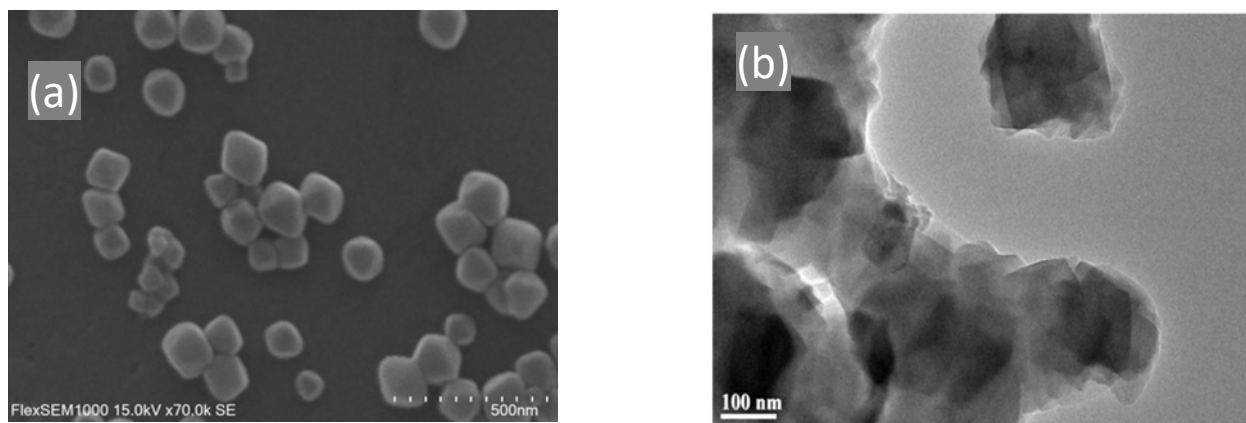


Figure 6. SEM images of (a) UiO-66 and TEM images of (b) UiO-66.

3.7. Catalytic and Reduction Reaction Kinetics Activity Study of Nano UiO-66 MOF

An often-studied model reduction reaction, i.e., the reduction of 4-NP to 4-AP, was evaluated using our synthesized nano MOF catalyst by using a minimum amount of sodium borohydride as a reducer. This catalytic reduction is considered a model catalytic process because it is often used to evaluate the catalytic efficiency of noble metal nano-particles [37]. The catalytic efficiency of noble metal nano-particles highly depends on their strong interactions with 4-NP and the interfacial surface area. Thus, MOFs are an ideal

choice, with a high metal concentration at their core and with an exuberant surface area. UV-vis spectra for 4-nitrophenol, 4-nitrophenoxide and 4-aminophenol is shown in Figure S2. Similarly, UV-vis spectra for UiO-6, UiO-66-NO₂ and UiO-66-NH₂ is shown in Figure S3. To understand the reduction process, sequential details of the experiments conducted, and the subsequent results are discussed as follows: (a) aqueous solution of 4-NP (3 mL, 25 mg L⁻¹) was mixed with the reducer NaBH₄ (3 mg) in a quartz cell, and shortly after the mixing, there was a color change of yellow to green, which is shown in Figure 7—indicating the formation of phenolate ions. These color changes were accompanied by a spectral shift in the absorption peak from 320 nm (4-Nitrophenol) to 400 nm (4-Nitrophenolate). Excess sodium borohydride was used to shift the equilibrium in the favor of phenolate ions [18,38]. The intensity of the UV-Vis peak remained unchanged until the catalyst was added to the reaction mixture; (b) The catalytic reduction of 4-Nitrophenol started on addition of the catalyst (dispersed in a mass to volume ratio of 1 mg/1 mL of water) to the cuvette. The steady decrease of the intensity of the absorption peak at 400 nm, which corresponds to 4-NP, and the appearance of a new peak at 300 nm, corresponding to 4-Aminophenol, and its continuous increase evidenced the progressive reduction process; (c) The peak associated to 4-NP disappeared after 540 s, 480 s, and 300 s from the start of the reaction for 0.2, 0.3, 0.5 mg of the UiO-66 catalyst. These results confirmed the complete reduction of 4-NP in the reaction mixture. The intensity of the absorption peak at around 300 nm increased progressively, indicating that 4-AP gradually accumulated in the reaction mixture. These results confirmed that UiO-66 nano MOF particles acted as a catalyst in the reduction of 4-NP. Similarly, in the case of MOF-5 (Zn-BDC) and MIL-101, (Fe-BDC) MOFs did not show catalytic activity—which is shown in Figures 8 and 9. Generally, the reduction reactions depend on the concentration of the catalyst, so we examined the reduction process with different quantities (0.2 mg/mL, 0.3 mg/mL, 0.5 mg/mL) of catalyst to obtain an optimum reduction rate.

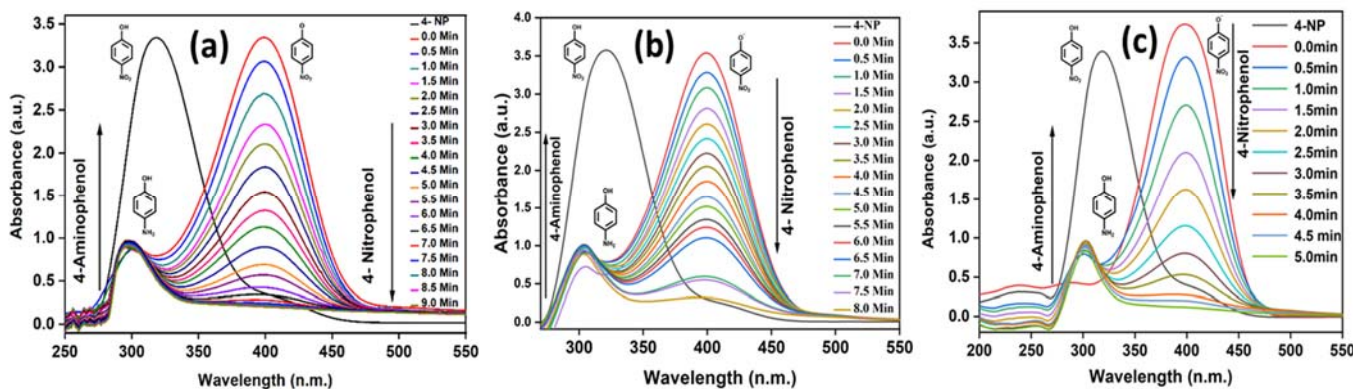


Figure 7. UV-Vis spectra of the catalytic reduction of 4-NP to 4-AP at different reaction times and different concentrations of UiO-66: (a) 0.2 mg, (b) 0.3 mg, and (c) 0.5 mg. The absorbance peak at 300, 317, and 400 nm corresponds to 4-AP, Phenolate ion, and 4-NP, respectively. On addition of UiO-66 nano particles, the intensity of the absorption peak at 400 nm started decreasing, whereas the peak at 300 nm started increasing, indicating the progress of the catalytic reduction.

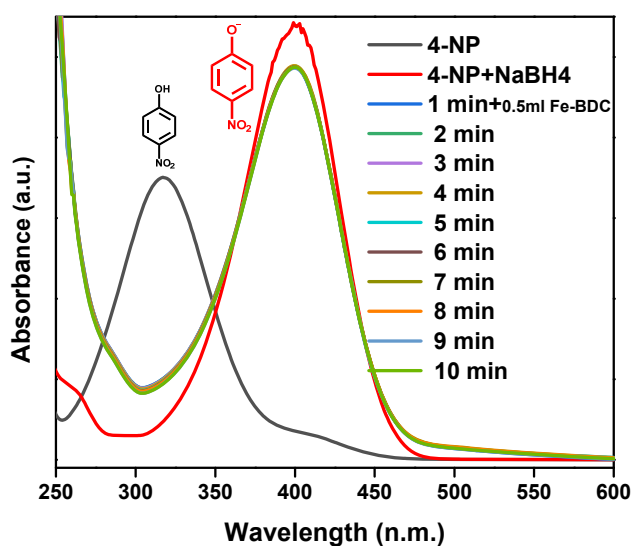


Figure 8. UV-Vis spectra of the catalytic reduction of 4-NP to 4-AP using 0.5 mg of (Fe-BDC) catalyst.

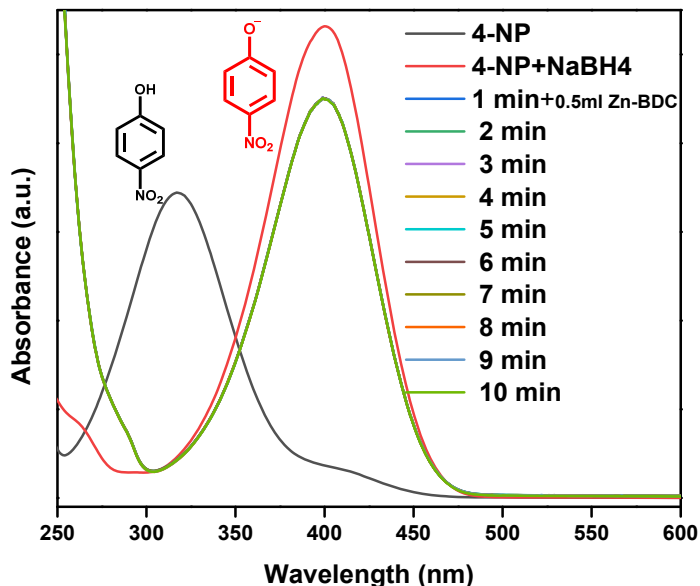


Figure 9. UV-Vis spectra of the catalytic reduction of 4-NP to 4-AP using 0.5 mg of (Zn-BDC).

Assuming a pseudo-first-order reaction, the following equation was considered to evaluate the kinetic parameters.

$$\ln\left(\frac{A_t}{A_0}\right) = \ln\left(\frac{C_t}{C_0}\right) = kt \quad (1)$$

where C_t is the concentration at time t , C_0 is the concentration at time 0, and k is the rate constant.

The linear fitting of the experimental data is shown in Figure 10. The rate constants were determined from fitting to the plot $\ln(A_t/A_0)$ and are shown in Table 1. A good correlation in the linear fitting was obtained, and the rate constants were determined to be 0.230, 0.303, and 0.367 S^{-1} for 0.2, 0.3 and 0.5 mg of the catalysts, respectively.

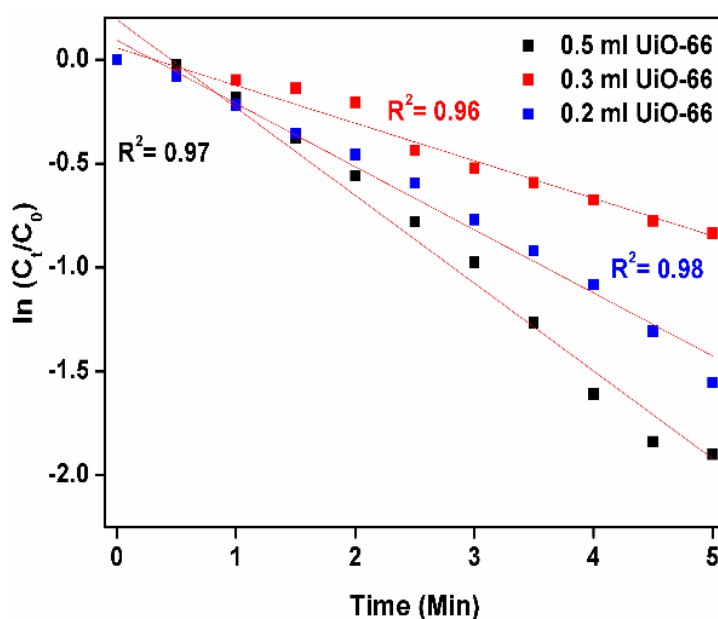


Figure 10. Pseudo first-order linear fitting to the intensity of the time variant UV-Vis spectra, obtained throughout the catalytic reduction of 4-NP to 4-AP.

Table 1. The rate constant values at different UiO-66 catalyst concentrations.

Catalyst	Quantity (mg)	First-Order, k_1 (S^{-1})	Time (min)
UIO-66	0.5	0.23	5
	0.3	0.303	8
	0.2	0.367	9

3.8. Reusability Study of the UiO-66 Nano MOF

For a check on the stability and reusability of the catalyst UIO-66, the MOF catalyst was washed, dried, and reused for five consecutive cycles following the same experimental conditions as shown in Figure 11. The PXRD of the pristine and the recovered UIO-66 MOF after catalysis is depicted in Figure S4. The catalytic efficiency of this nano MOF was compared with other metal composite catalysts and is summarized in Table 2. In this study, 0.5 mg of UiO-66 was used to reduce 0.3 mM of 4-NP in 300 s of reaction time, which can be simplified to a standard value of to 2×10^{-3} mM of 4-NP per mg of catalyst per second, whereas other noble metal-based catalysts such as PtCoY and Au-mSiO₂ catalyze 3.89×10^{-5} and 2.53×10^{-3} mM of 4-Nitrophenol to 4-Aminophenol per mg per second, respectively [38].

In a simple comparison, it can be noticed that our catalyst is better, or at least on a similar scale to other composite noble metal-based catalysts [39]. Furthermore, the stability and recyclability of UiO-66 MOFs are one of its kind in the family of MOFs and catalysts [40]. This result suggests that UiO-66 can be used as a model catalyst in catalytic reduction reactions.

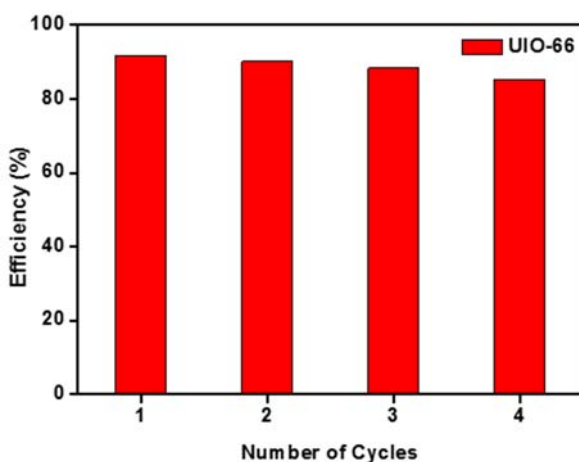


Figure 11. Reduction efficiency of UiO-66 catalysts for catalytic reduction of 4-NP to 4-AP under similar experimental conditions.

Table 2. Table showing the catalytic performance of different catalysts.

Catalyst	Catalyst Used	Reaction Rate Constants Per Unit	Reference
PtCoY Composite	20 mg	3.89	[41]
Ag-MMT	10 mg	3.33	[42]
Ag@CTGU-3	1 mg	8.64	[43]
Au NPs	1 mL	0.51	[44]
Ag/POM-1	2 mg	3.65	[45]
Ag NPs/RGO-LShybrid	76 mg	1.893	[46]
Co@N-C from ZIF-67	0.1 mg	1.25	[40]
UiO-66-NH ₂ /TTACP/Ni@Pd	1.0 mg	1.42×10^{-2}	[17]
UiO-66	0.2	0.364	This work

3.9. Proposed Mechanism of the Reduction Reaction by the UiO-66 Nano MOF

To understand the mechanism of the reduction reaction, ¹H NMR of 4-NP and 4-AP before and after the reaction were examined with three nano MOFs, UiO-66, UiO-66-NO₂ and UiO-66-NH₂ (Figures S5–S8). In addition, ESI-MS spectrum of the reaction mixture before and after the catalysis were examined (Figures S9 and S10). The unique catalytic activity of UiO-66 may be attributed to the Lewis acidic nature of the metal nodes of the framework molecules. Furthermore, UiO-66 MOF is material well known for its adsorption behavior helping in adhering P-Nitrophenol anions onto the MOF's surface [47–49]. The reducing agents, borohydride ions, are adsorbed onto the MOF nano particles' surfaces. The Zr-cluster in UiO-66 MOF, with high a tendency to attract electrons—owing to its Lewis acidic behavior—as compared to MOF-5 (Zn-BDC) and MIL-101 (Fe-BDC), acts as an electron acceptor. Upon adsorption of P-Nitrophenol on the MOF surfaces via electrostatic interactions, the charge transfer occurs between the nano MOF and the Nitrophenol. The uptake of the excess electron in the MOF clusters eventually leads to the reduction of 4-Nitrophenol to 4-Aminophenol. In the case of UiO-66-NH₂ and UiO-66-NO₂, the presence of additional groups on the ligand affect the thermal and chemical stability, as well as the electronic properties of the active site. The additional functional groups increase the Bronsted acidity of the materials and decrease the Lewis acidity. Therefore, the decrease in the Lewis acidity of UiO-66-NH₂ and UiO-66-NO₂ in comparison to UiO-66 is the main reason for their inactiveness during this reduction reaction. In addition, the presence of additional groups creates steric crowding that prevents the incoming substrate (para nitrophenol) from interacting with the Zr sites. It has been reported that ZrO₂ and Ni, Cu, and Zn-doped ZrO₂ have been used for the reduction of 4-NP. However, the ZrO₂ did not achieve a good catalytic activity as compared to the UiO-66 MOF. The catalytic conversation time was around 90 min for ZrO₂, which is very long compared to the catalytic conversion time of the UiO-66 MOF.

time of 10 min with the UiO-66. The efficacy and reusability of the UiO-66 catalyst indicate a near-perfect adsorption–desorption process in this system.

4. Conclusions

A robust UiO-66 nano MOF was successfully synthesized and characterized by PXRD, Diffused Reflectance UV-Vis, FT-IR, TGA, SEM, and TEM analysis. The nano-scaled MOF was utilized as a catalyst to catalyze Nitroarenes to Aminoarenes, a model reduction reaction widely considered in academia and industries, and was also compared with other two type of MOFs—namely, MOF-5 (Zn-BDC) and MIL-101 (Fe-BDC). This noble Lewis acid-containing metal catalyst was novel due to being stable under operative conditions owing to their strong reticular structure, which also enables them to be reused multiple times. Furthermore, they do not need to be tailored for catalytic reduction, as is often observed in other catalysts. Together with their nontoxic behavior, easy mass-scale synthesis, and optimum catalytic activity and recyclability, they can serve as a model catalyst in reduction reactions.

Supplementary Materials: The following are available online at <https://www.mdpi.com/article/10.3390/catal12050494/s1>, Figure S1: PXRD patterns of MIL-101(Fe) and MOF-5; Figure S2: UV-vis spectra for 4-nitrophenol (black line) 4-nitrophenoxide (red line) and 4-aminophenol (blue line) in solutions; Figure S3: UV-vis spectra for UiO-66 (black line) UiO-66-NO₂ (red line) and UiO-66-NH₂ (blue line) in solutions; Figure S4: XRD of UiO-66 as-synthesized and after catalysis; Figure S5: ¹H NMR spectra of reactant before the reaction showing the 4-NP peak; Figure S6: ¹H NMR spectra of product after the reaction showing the 4-AP peak using UiO-66 as catalyst; Figure S7: ¹H NMR spectra of product after the reaction showing the absence of 4-AP peak at (5.0 ppm) using UiO-66-NO₂ as catalyst; Figure S8: ¹H NMR spectra of product after the reaction showing the absence of 4-AP peak at (5.0 ppm) using UiO-66-NH₂ as catalyst; Figure S9: ESI-MS spectrum in negative ion mode of an aliquot taken before reaction in the presence of NaBH₄ and 4-NP; Figure S10: ESI-MS spectrum in positive ion mode of an aliquot taken after reaction in the presence of UiO-66.

Author Contributions: Conceptualization, J.P.; methodology, J.P.; software, J.P.; validation, J.P., H.S.J., R.S. (Raghabendra Samantray) and R.S. (Rojalin Sahu); formal analysis, S.P.B.; investigation, J.P. and S.P.B.; resources, R.S. (Raghabendra Samantray) and R.S. (Rojalin Sahu); data curation, J.P. and A.M.; writing—original draft preparation, J.P. and S.P.B.; writing—review and editing, J.P., S.P.B., A.M., H.S.J., R.S. (Raghabendra Samantray) and R.S. (Rojalin Sahu); visualization, J.P. and R.S. (Rojalin Sahu); supervision, H.S.J., R.S. (Raghabendra Samantray) and R.S. (Rojalin Sahu); project administration, H.S.J., R.S. (Raghabendra Samantray) and R.S. (Rojalin Sahu); funding acquisition, H.S.J., R.S. (Raghabendra Samantray) and R.S. (Rojalin Sahu). All authors have read and agreed to the published version of the manuscript.

Funding: The study is partially supported by a Birac Ignition Grant, Department of Biotechnology, India (Grant No.: BIRAC/KIIT0023/BIG-05/14).

Data Availability Statement: This study did not report any data.

Acknowledgments: We would like to thank P. V. Satyam for his kind help in measuring the TEM images of our samples.

Conflicts of Interest: The authors declare no conflict of interest.

References

1. Mallick, A.; El-Zohry, A.M.; Shekhah, O.; Yin, J.; Jia, J.; Aggarwal, H.; Emwas, A.-H.; Mohammed, O.F.; Eddaoudi, M. Unprecedented Ultralow Detection Limit of Amines using a Thiadiazole-Functionalized Zr(IV)-Based Metal-Organic Framework. *J. Am. Chem. Soc.* **2019**, *141*, 7245–7249. [[CrossRef](#)] [[PubMed](#)]
2. Nguyen, H.G.T.; Schweitzer, N.M.; Chang, C.-Y.; Drake, T.L.; So, M.C.; Stair, P.C.; Farha, O.K.; Hupp, J.T.; Nguyen, S.T. Vanadium-Node-Functionalized UiO-66: A Thermally Stable MOF-Supported Catalyst for the Gas-Phase Oxidative Dehydrogenation of Cyclohexene. *ACS Catal.* **2014**, *4*, 2496–2500. [[CrossRef](#)]
3. Jiao, L.; Wang, Y.; Jiang, H.-L.; Xu, Q. Metal-Organic Frameworks as Platforms for Catalytic Applications. *Adv. Mater.* **2018**, *30*, e1703663. [[CrossRef](#)] [[PubMed](#)]

4. Wang, C.; Liu, X.; Keser Demir, N.; Chen, J.P.; Li, K. Applications of water stable metal-organic frameworks. *Chem. Soc. Rev.* **2016**, *45*, 5107–5134. [[CrossRef](#)] [[PubMed](#)]
5. Zhao, X.; Wang, Y.; Li, D.-S.; Bu, X.; Feng, P. Metal-Organic Frameworks for Separation. *Adv. Mater.* **2018**, *30*, e1705189. [[CrossRef](#)] [[PubMed](#)]
6. Herbst, A.; Khutia, A.; Janiak, C. Brønsted instead of Lewis acidity in functionalized MIL-101Cr MOFs for efficient heterogeneous (nano-MOF) catalysis in the condensation reaction of aldehydes with alcohols. *Inorg. Chem.* **2014**, *53*, 7319–7333. [[CrossRef](#)]
7. Dhakshinamoorthy, A.; Santiago-Portillo, A.; Asiri, A.M.; Garcia, H. Engineering UiO-66 Metal Organic Framework for Heterogeneous Catalysis. *ChemCatChem* **2019**, *11*, 899–923. [[CrossRef](#)]
8. Kuppler, R.J.; Timmons, D.J.; Fang, Q.-R.; Li, J.-R.; Makal, T.A.; Young, M.D.; Yuan, D.; Zhao, D.; Zhuang, W.; Zhou, H.-C. Potential applications of metal-organic frameworks. *Coord. Chem. Rev.* **2009**, *293*, 3042–3066. [[CrossRef](#)]
9. Furukawa, H.; Ko, N.; Go, Y.B.; Aratani, N.; Choi, S.B.; Choi, E.; Yazaydin, A.O.; Snurr, R.Q.; O’Keeffe, M.; Kim, J.; et al. Ultrahigh porosity in metal-organic frameworks. *Science* **2010**, *329*, 424–428. [[CrossRef](#)]
10. Li, P.; Vermeulen, N.A.; Malliakas, C.D.; Gómez-Gualdrón, D.A.; Howarth, A.J.; Mehdi, B.L.; Dohnalkova, A.; Browning, N.D.; O’Keeffe, M.; Farha, O.K. Bottom-up construction of a superstructure in a porous uranium-organic crystal. *Science* **2017**, *356*, 624–627. [[CrossRef](#)]
11. Farha, O.K.; Eryazici, I.; Jeong, N.C.; Hauser, B.G.; Wilmer, C.E.; Sarjeant, A.A.; Snurr, R.Q.; Nguyen, S.T.; Yazaydin, A.Ö.; Hupp, J.T. Metal-organic framework materials with ultrahigh surface areas: Is the sky the limit? *J. Am. Chem. Soc.* **2012**, *134*, 15016–15021. [[CrossRef](#)] [[PubMed](#)]
12. Grünker, R.; Bon, V.; Müller, P.; Stoeck, U.; Krause, S.; Mueller, U.; Senkovska, I.; Kaskel, S. A new metal-organic framework with ultra-high surface area. *Chem. Commun.* **2014**, *50*, 3450–3452. [[CrossRef](#)] [[PubMed](#)]
13. Dhakshinamoorthy, A.; Garcia, H. Catalysis by metal nanoparticles embedded on metal-organic frameworks. *Chem. Soc. Rev.* **2012**, *41*, 5262–5284. [[CrossRef](#)] [[PubMed](#)]
14. Li, T.-T.; Liu, Y.-M.; Wang, T.; Wu, Y.-L.; He, Y.-L.; Yang, R.; Zheng, S.-R. Regulation of the surface area and surface charge property of MOFs by multivariate strategy: Synthesis, characterization, selective dye adsorption and separation. *Microporous Mesoporous Mater.* **2018**, *272*, 101–108. [[CrossRef](#)]
15. Zong, M.-Y.; Fan, C.-Z.; Yang, X.-F.; Wang, D.-H. Promoting Ni-MOF with metallic Ni for highly-efficient p-nitrophenol hydrogenation. *Mol. Catal.* **2021**, *509*, 111609. [[CrossRef](#)]
16. Agarwal, R.A.; Gupta, A.K.; De, D. Flexible Zn-MOF Exhibiting Selective CO₂ Adsorption and Efficient Lewis Acidic Catalytic Activity. *Cryst. Growth Des.* **2019**, *19*, 2010–2018. [[CrossRef](#)]
17. Sadeghzadeh, S.M.; Zhiani, R.; Emrani, S. The reduction of 4-nitrophenol and 2-nitroaniline by the incorporation of Ni@Pd MNPs into modified UiO-66-NH₂ metal-organic frameworks (MOFs) with tetrathia-azacyclopentadecane. *New J. Chem.* **2018**, *42*, 988–994. [[CrossRef](#)]
18. Xu, X.; Li, H.; Xie, H.; Ma, Y.; Chen, T.; Wang, J. Zinc cobalt bimetallic nanoparticles embedded in porous nitrogen-doped carbon frameworks for the reduction of nitro compounds. *J. Mater. Res.* **2017**, *32*, 1777–1786. [[CrossRef](#)]
19. Rani, P.; Srivastava, R. Nucleophilic addition of amines, alcohols, and thiophenol with epoxide/olefin using highly efficient zirconium metal organic framework heterogeneous catalyst. *RSC Adv.* **2015**, *5*, 28270–28280. [[CrossRef](#)]
20. Xie, K.; He, Y.; Zhao, Q.; Shang, J.; Gu, Q.; Qiao, G.G.; Webley, P.A. Pd(0) loaded Zn₂(azoBDC)₂(dabco) as a heterogeneous catalyst. *CrystEngComm* **2017**, *19*, 4182–4186. [[CrossRef](#)]
21. Hinde, C.S.; Webb, W.R.; Chew, B.K.J.; Tan, H.R.; Zhang, W.-H.; Hor, T.S.A.; Raja, R. Utilisation of gold nanoparticles on amine-functionalised UiO-66 (NH₂-UiO-66) nanocrystals for selective tandem catalytic reactions. *Chem. Commun.* **2016**, *52*, 6557–6560. [[CrossRef](#)] [[PubMed](#)]
22. Cheng, S.; Shang, N.; Zhou, X.; Feng, C.; Gao, S.; Wang, C.; Wang, Z. High catalytic activity of a bimetallic AgPd alloy supported on UiO-66 derived porous carbon for transfer hydrogenation of nitroarenes using formic acid-formate as the hydrogen source. *New J. Chem.* **2017**, *41*, 9857–9865. [[CrossRef](#)]
23. Yin, D.; Li, C.; Ren, H.; Liu, J.; Liang, C. Gold-Palladium-Alloy-Catalyst Loaded UiO-66-NH₂ for Reductive Amination with Nitroarenes Exhibiting High Selectivity. *ChemistrySelect* **2018**, *3*, 5092–5097. [[CrossRef](#)]
24. Gole, B.; Sanyal, U.; Mukherjee, P.S. A smart approach to achieve an exceptionally high loading of metal nanoparticles supported by functionalized extended frameworks for efficient catalysis. *Chem. Commun.* **2015**, *51*, 4872–4875. [[CrossRef](#)] [[PubMed](#)]
25. Gao, G.; Xi, Q.; Zhang, Y.; Jin, M.; Zhao, Y.; Wu, C.; Zhou, H.; Guo, P.; Xu, J. Atomic-scale engineering of MOF array confined Au nanoclusters for enhanced heterogeneous catalysis. *Nanoscale* **2019**, *11*, 1169–1176. [[CrossRef](#)]
26. Zhang, H.; Qi, S.; Niu, X.; Hu, J.; Ren, C.; Chen, H.; Chen, X. Metallic nanoparticles immobilized in magnetic metal-organic frameworks: Preparation and application as highly active, magnetically isolable and reusable catalysts. *Catal. Sci. Technol.* **2014**, *4*, 3013–3024. [[CrossRef](#)]
27. Abdelhamid, H.N. High performance and ultrafast reduction of 4-nitrophenol using metal-organic frameworks. *J. Environ. Chem. Eng.* **2021**, *9*, 104404. [[CrossRef](#)]
28. Panda, J.; Sahu, S.N.; Sahoo, J.K.; Biswal, S.P.; Pattanayak, S.K.; Samantaray, R.; Sahu, R. Efficient removal of two anionic dyes by a highly robust zirconium based metal organic framework from aqueous medium: Experimental findings with molecular docking study. *Environ. Nanotechnol. Monit. Manag.* **2020**, *14*, 100340. [[CrossRef](#)]

29. Katz, M.J.; Brown, Z.J.; Colón, Y.J.; Siu, P.W.; Scheidt, K.A.; Snurr, R.Q.; Hupp, J.T.; Farha, O.K. A facile synthesis of UiO-66, UiO-67 and their derivatives. *Chem. Commun.* **2013**, *49*, 9449–9451. [[CrossRef](#)]
30. Hendrickx, K.; Vanpoucke, D.E.P.; Leus, K.; Lejaeghere, K.; van Yperen-De Deyne, A.; van Speybroeck, V.; van der Voort, P.; Hemelsoet, K. Understanding Intrinsic Light Absorption Properties of UiO-66 Frameworks: A Combined Theoretical and Experimental Study. *Inorg. Chem.* **2015**, *54*, 10701–10710. [[CrossRef](#)]
31. Kandiah, M.; Nilsen, M.H.; Usseglio, S.; Jakobsen, S.; Olsbye, U.; Tilset, M.; Larabi, C.; Quadrelli, E.A.; Bonino, F.; Lillerud, K.P. Synthesis and Stability of Tagged UiO-66 Zr-MOFs. *Chem. Mater.* **2010**, *22*, 6632–6640. [[CrossRef](#)]
32. Massoudinejad, M.; Ghaderpoori, M.; Shahsavani, A.; Amini, M.M. Adsorption of fluoride over a metal organic framework Uio-66 functionalized with amine groups and optimization with response surface methodology. *J. Mol. Liq.* **2016**, *221*, 279–286. [[CrossRef](#)]
33. Shen, L.; Liang, S.; Wu, W.; Liang, R.; Wu, L. Multifunctional NH₂-mediated zirconium metal-organic framework as an efficient visible-light-driven photocatalyst for selective oxidation of alcohols and reduction of aqueous Cr(VI). *Dalton Trans.* **2013**, *42*, 13649–13657. [[CrossRef](#)] [[PubMed](#)]
34. Shen, L.; Liang, R.; Luo, M.; Jing, F.; Wu, L. Electronic effects of ligand substitution on metal-organic framework photocatalysts: The case study of UiO-66. *Phys. Chem. Chem. Phys.* **2015**, *17*, 117–121. [[CrossRef](#)]
35. Ghani, M.; Font Picó, M.F.; Salehinia, S.; Palomino Cabello, C.; Maya, F.; Berlier, G.; Saraji, M.; Cerdà, V.; Turnes Palomino, G. Metal-organic framework mixed-matrix disks: Versatile supports for automated solid-phase extraction prior to chromatographic separation. *J. Chromatogr. A* **2017**, *1488*, 1–9. [[CrossRef](#)]
36. Zhu, X.; Gu, J.; Wang, Y.; Li, B.; Li, Y.; Zhao, W.; Shi, J. Inherent anchorages in UiO-66 nanoparticles for efficient capture of alendronate and its mediated release. *Chem. Commun.* **2014**, *50*, 8779–8782. [[CrossRef](#)] [[PubMed](#)]
37. Navalón, S.; Álvaro, M.; Dhakshinamoorthy, A.; García, H. Encapsulation of Metal Nanoparticles within Metal-Organic Frameworks for the Reduction of Nitro Compounds. *Molecules* **2019**, *24*, 3050. [[CrossRef](#)]
38. Satapathy, S.; Mohanta, J.; Si, S. Modulating the Catalytic Activity of Gold Nanoparticles through Surface Tailoring. *ChemistrySelect* **2016**, *1*, 4940–4948. [[CrossRef](#)]
39. Krishna, R.; Fernandes, D.M.; Ventura, J.; Freire, C.; Titus, E. Facile synthesis of reduced graphene oxide supported Pd@NixB/RGO nanocomposite: Novel electrocatalyst for ethanol oxidation in alkaline media. *Int. J. Hydrogen Energy* **2016**, *41*, 11811–11822. [[CrossRef](#)]
40. Yusran, Y.; Xu, D.; Fang, Q.; Zhang, D.; Qiu, S. MOF-derived Co@N-C nanocatalyst for catalytic reduction of 4-nitrophenol to 4-aminophenol. *Microporous Mesoporous Mater.* **2017**, *241*, 346–354. [[CrossRef](#)]
41. El-Bahy, Z.M. Preparation and characterization of Pt-promoted NiY and CoY catalysts employed for 4-nitrophenol reduction. *Appl. Catal. A Gen.* **2013**, *468*, 175–183. [[CrossRef](#)]
42. Praus, P.; Turicová, M.; Karlíková, M.; Kvítek, L.; Dvorský, R. Nanocomposite of montmorillonite and silver nanoparticles: Characterization and application in catalytic reduction of 4-nitrophenol. *Mater. Chem. Phys.* **2013**, *140*, 493–498. [[CrossRef](#)]
43. Wu, X.-Q.; Huang, D.-D.; Zhou, Z.-H.; Dong, W.-W.; Wu, Y.-P.; Zhao, J.; Li, D.-S.; Zhang, Q.; Bu, X. Ag-NPs embedded in two novel Zn₃/Zn₅-cluster-based metal-organic frameworks for catalytic reduction of 2/3/4-nitrophenol. *Dalton Trans.* **2017**, *46*, 2430–2438. [[CrossRef](#)] [[PubMed](#)]
44. Lawrence, R.L.; Scola, B.; Li, Y.; Lim, C.-K.; Liu, Y.; Prasad, P.N.; Swihart, M.T.; Knecht, M.R. Remote Optically Controlled Modulation of Catalytic Properties of Nanoparticles through Reconfiguration of the Inorganic/Organic Interface. *ACS Nano* **2016**, *10*, 9470–9477. [[CrossRef](#)] [[PubMed](#)]
45. Yang, X.-J.; Sun, M.; Zang, H.-Y.; Ma, Y.-Y.; Feng, X.-J.; Tan, H.-Q.; Wang, Y.-H.; Li, Y.-G. Hybrid Coordination Networks Constructed from ϵ -Keggin-Type Polyoxometalates and Rigid Imidazole-Based Bridging Ligands as New Carriers for Noble-Metal Catalysts. *Chem. Asian J.* **2016**, *11*, 858–867. [[CrossRef](#)]
46. Liu, Y.Y.; Zhao, Y.H.; Zhou, Y.; Guo, X.L.; Chen, Z.T.; Zhang, W.J.; Zhang, Y.; Chen, J.; Wang, Z.M.; Sun, L.T.; et al. High-efficient catalytic reduction of 4-nitrophenol based on reusable Ag nanoparticles/graphene-loading loofah sponge hybrid. *Nanotechnology* **2018**, *29*, 315702. [[CrossRef](#)]
47. Strachan, J.; Barnett, C.; Masters, A.F.; Maschmeyer, T. 4-Nitrophenol Reduction: Probing the Putative Mechanism of the Model Reaction. *ACS Catal.* **2020**, *10*, 5516–5521. [[CrossRef](#)]
48. Guan, Q.; Wang, B.; Chai, X.; Liu, J.; Gu, J.; Ning, P. Comparison of Pd-UiO-66 and Pd-UiO-66-NH₂ catalysts performance for phenol hydrogenation in aqueous medium. *Fuel* **2017**, *205*, 130–141. [[CrossRef](#)]
49. Yang, Q.; Zhang, H.-Y.; Wang, L.; Zhang, Y.; Zhao, J. Ru/Uio-66 Catalyst for the Reduction of Nitroarenes and Tandem Reaction of Alcohol Oxidation/Knoevenagel Condensation. *ACS Omega* **2018**, *3*, 4199–4212. [[CrossRef](#)]